Searching for axionlike time-dependent cosmic birefringence with data from SPT-3G

```
K. R. Ferguson, <sup>1,*</sup> A. J. Anderson, <sup>2,3,4</sup> N. Whitehorn, <sup>5,1</sup> P. A. R. Adé, M. Archipley, <sup>7,8</sup> J. S. Avva, L. Balkenhol, <sup>10</sup> K. Benabed, <sup>1</sup> A. N. Benden, <sup>12,3</sup> B. A. Benson, <sup>2,3,4</sup> F. Bianchini, <sup>13,14,15</sup> L. E. Bleem, <sup>12,3</sup> F. R. Bouchet, <sup>11</sup> L. Bryant, <sup>16</sup> E. Camphuis, <sup>1</sup> J. E. Carlstron, <sup>16,17,12,4</sup> T. W. Cecib, <sup>12</sup> C. L. Chang, <sup>12,3,4</sup> P. Chaubal, <sup>0</sup> P. M. Chichura, <sup>17,3</sup> T.-L. Chou, <sup>17,3</sup> T. M. Crawford, <sup>3,4</sup> A. Cukierman, <sup>13,15,14</sup> C. Daley, <sup>7</sup> T. de Haan, <sup>8</sup> K. R. Dibert, <sup>4,3</sup> M. A. Dobbs, <sup>19,20</sup> A. Doussot, <sup>1</sup> D. Dutchen, <sup>21</sup> W. Everett, <sup>2</sup> C. Feng, <sup>3</sup> A. Fosten, <sup>24</sup> S. Galli, <sup>11</sup> A. E. Gambrei, <sup>3</sup> R. W. Gardner, <sup>16</sup> N. Goeckner-Wald, <sup>4,13</sup> R. Gualtieri, <sup>12</sup> F. Guidi, <sup>11</sup> S. Guns, <sup>9</sup> N. W. Halverson, <sup>25,26</sup> E. Hivon, <sup>11</sup> G. P. Holden, <sup>23</sup> W. L. Holzapfel, J. C. Hood, N. Huang, L. Knox, <sup>27</sup> M. Korman, <sup>24</sup> C.-L. Kuo, <sup>13,14,15</sup> A. T. Lee, <sup>9,28</sup> A. E. Lowitz, <sup>3</sup> C. Lu, <sup>23</sup> M. Millea, <sup>9</sup> J. Montgomery, <sup>9</sup> T. Natoli, <sup>3</sup> G. I. Noble, <sup>9</sup> V. Novosad, <sup>9</sup> Y. Omori, <sup>3</sup> S. Padin, <sup>3,30</sup> Z. Pan, <sup>12,3,17</sup> P. Paschos, K. Prabhu, <sup>7</sup> W. Quan, <sup>17,3</sup> A. Rahlin, <sup>2,3</sup> C. L. Reichard, <sup>10</sup> M. Rouble, <sup>19</sup> J. E. Ruh, <sup>2</sup> E. Schiappuccl, <sup>0</sup> G. Smeche, J. A. Sobrin, <sup>17,3</sup> J. Stephen, <sup>6</sup> A. Suzuki, <sup>8</sup> C. Tandoi, <sup>7</sup> K. L. Thompson, <sup>13,14,15</sup> B. Thorne, <sup>7</sup> C. Tucker, <sup>6</sup> C. Umilta, <sup>23</sup> J. D. Vieira, <sup>7,23,8</sup> G. Wang, <sup>12</sup> W. L. K. Wuo, <sup>13,15</sup> V. Yefremenko, <sup>12</sup> and M. R. Young, <sup>2</sup>
```

```
(SPT-3G Collaboration)
<sup>1</sup>Departmentof Physics and AstronomyUniversity of California, Los Angeles California 90095, USA
    <sup>2</sup>Fermi NationalAccelerator LaboratoryMS209,P.O. Box 500,Batavia,Illinois 60510,USA
                  <sup>3</sup>Kavli Institute for CosmologicaPhysics,University of Chicago,
                       5640 South Ellis AvenueChicago, Illinois 60637, USA
                 <sup>4</sup>Department of Astronomy and Astrophysics Iniversity of Chicago,
                       5640 South Ellis AvenueChicago, Illinois 60637, USA
<sup>5</sup>Department of Physics and Astronomy, Michigan State University, East Lansing, Michigan 48824, USA
     <sup>6</sup>Schoolof Physics and AstronomyCardiff University, Cardiff CF24 3YB, United Kingdom
                <sup>7</sup>Departmentof Astronomy,University of Illinois Urbana-Champaign,
                        1002 WestGreen Street Urbana, Illinois 61801, USA
        <sup>8</sup>Center for AstroPhysicaSurveys,National Center for Supercomputing Applications,
                                    Urbana, Illinois 61801, USA
          <sup>9</sup>Departmentof Physics, University of California, Berkeley, California 94720, USA
           <sup>10</sup>Schoolof Physics, University of Melbourne, Parkville, Victoria 3010, Australia
            <sup>11</sup>Institut d'Astrophysique de ParisUMR 7095, CNRS & Sorbonne Universit
                            98 bis boulevard Arago,75014 Paris, France
                    <sup>12</sup>High-Energy Physics DivisionArgonne NationalLaboratory,
                       9700 South Cass Avenueemont, Illinois 60439, USA
            <sup>13</sup>Kavli Institute for Particle Astrophysics and Cosmologytanford University,
                         452 Lomita Mall, Stanford, California 94305, USA
<sup>14</sup>Department ofPhysics,Stanford University,382 Via Pueblo Mall,Stanford,California 94305,USA
<sup>15</sup>SLAC NationalAccelerator Laboratory 2575 Sand Hill Road, Menlo Park, California 94025, USA
<sup>16</sup>Enrico Fermi Institute, University of Chicago, 5640 South Ellis Avenue, Chicago, Illinois 60637, USA
<sup>17</sup>Department of Physics, University of Chicago, 5640 South Ellis Avenue, Chicago, Illinois 60637, USA
     High Energy Accelerator Research Organization (KER)sukuba Ibaraki 305-0801, Japan
                <sup>19</sup>Departmentof Physics and McGillSpace InstituteMcGill University,
                      3600 Rue UniversityMontreal, Quebec H3A 2T8Canada
 <sup>20</sup>Canadian Institute for Advanced Resear@IFAR Program in Gravity and the Extreme Universe,
                                 Toronto, Ontario M5G 1Z8, Canada
             <sup>21</sup>Joseph Henry Laboratories d hysics, Jadwin Hall, Princeton University,
                                 Princeton, New Jersey 08544USA
           <sup>22</sup>Departmentof Astrophysicaland Planetary Sciences Iniversity of Colorado,
                                   Boulder, Colorado 80309.USA
                 <sup>23</sup>Departmentof Physics, University of Illinois Urbana-Champaign,
                        1110 WestGreen Street Urbana, Illinois 61801, USA
      <sup>24</sup>Departmentof Physics,Case Western Reserve Universityleveland,Ohio 44106,USA
        <sup>25</sup>CASA, Department of Astrophysical and Planetary Science Iniversity of Colorado,
                                   Boulder, Colorado 80309, USA
          <sup>26</sup>Departmentof Physics, University of Colorado, Boulder, Colorado 80309, USA
```

²⁷Department of Physics and Astronom University of California, One Shields Avenu@avis, California 95616, USA ²⁸Physics DivisionLawrence Berkeley Nationalaboratory, Berkeley, California 94720, USA ²⁹Materials Sciences DivisiorArgonne NationalLaboratory, 9700 South Cass Avenueemont, Illinois 60439, USA ³⁰California Institute of Technology, 1200 East California Boulevard, Pasadena, California 91125, USA ³¹Three-Speed Logidnc., Victoria, British Columbia V8S 3Z5Canada ³²David A. Dunlap Department Astronomy and Astrophysics Iniversity of Toronto, 50 St. George Street, Toronto, Ontario M5S 3H4, Canada

(Received 30 March 2022; accepted 15 July 2022phlished 29 August 2022)

Ultralight axionlike particles (ALPs) are compelling dark matter candidates because of their potential to resolve small-scale discrepancies between ACDM predictions and cosmologicalervationsAxionphoton coupling induces a polarization rotation in linearly polarized photons traveling through an ALP field; thus, as the local ALP dark matter field oscillates in time, distant static polarized sources will appear to oscillate with a frequency proportional to the ALP mass. We use observations of the cosmic microwave background from SPT-3G, the current receiver on the South Pole Telescope, to set upper limits on the value of the axion-photon coupling constant over the approximate mass range 24010-19 eV, corresponding to oscillation periods from 12 hours to 100 days. For periods between 1 and 100 days $(4.7 \times 10^{22} \text{ eV} \le \text{m}_{\phi} \le 4.7 \times 10^{20} \text{ eV})$, where the limit is approximately constant we set a median 95% C.L. upper limit on the amplitude of on-sky polarization rotation of 0.071 deg. Assuming that dark matter comprises a single ALP species with a local dark matter density of 0.3 GetViscororresponds to g $_{\phi\gamma}$ < 1.18 × 10⁻¹² GeV⁻¹ × $\check{\sigma}_{1.0 \times 10^{-21} \, \text{eV}}^{-1}$ Þ. These new limits representan improvement over the previous strongestmits set using the same effective a factor of ~3.8.

DOI: 10.1103/PhysRevD.106.042011

I. INTRODUCTION

Astrophysical observations have provided strong evidence for the existence of nonbaryonic dark matter [1,2]. problem [3–6], has emerged as a compelling dark matter g_{φγ} in narrow windows of mass within the favored range of candidate [7–11], although theoretical considerations constrain the region of mass parametespace it can lie in. Of broader astrophysical interest is a class of axionlike equations of motion in the form of an imaginary expoparticles (ALPs) that arise naturally in many string theory nential. The consequence of this is that posite-helicity models [12–14]. Although they couple to the Standard Model photon in much the same way as the QCD axion, ALPs do not solve the strong CP problemDespite this, they make promising dark matter candidates, as they may photon will be rotated by an amount proportional to the lie in a much wider region of parameter space than the highly constrained QCD axion [15,16]. For convenience, we will use "axion" as an umbrella term encompassing both the QCD axion and ALPs.

Many experiments have carried out axion searches. Generally these searches take advantagetbe coupling between axions and photons via the Primakoff effectly the presence of a strong magnetic field. Helioscope experdark matter candidate due to the long de Broglie wavements such as CAST [17] are able to set limits on the axidengths of their condensate fields their scale-dependent photon coupling constant g_{bv} across a wide range of

possible axion masses m_{ϕ} , with the upper mass range given by instrumental considerations rathethan a theoretical limit. Haloscopes like ADMX [18] and HAYSTAC The QCD axion, originally devised to solve the strong CP[19] instead use resonant cavities to set stringent limits on masses for the QCD axion.

The axion contributes an additional term to the photon photons pick up relative phase shifts as they travel through an axion field ([20], hereafter F19). From the point of view of an observer, the polarization angle of a linearly polarized difference between the axion field values at emission and absorption. Searches for this effect often focus on ultralight axions (those with masses roughly between 280eV and 10⁻¹⁸ eV) because cold axions with these masses form a Bose-Einstein condensate and thus behave as a classical field with a value that oscillates on human-observable timescales with periods in the range from hours to years. which an axion is converted into a photon (or vice versa) indditionally, ultralight axions are especially interesting as a clustering has the potentiato resolve long-standing discrepancies between observations and predictions of the standard cosmological model ACDM on small scales, such as the core/cusp problem and the too-big-to-fapiroblem [21,22]. Because thermally produced axions in this mass

Corresponding author. kferguson@physics.ucla.edu

range would still be relativistic today it is important that they be produced nonthermally for them to remain a viable that is, the fundamental statistical uncertainty or sample dark matter candidate. This may happen via vacuum realignment string decay or domain wall decay [10,23].

Using active galactic nuclei (AGN) as astrophysical polarization sources, Horns et al. [24] and Ivanov et al. [25] set limits on $g_{\Phi V}$ for ultralight axions. However, intrinsic variation in the polarization of AGN sources can oscillation effect. The BICEP/Keck collaboration has be difficult to disentangle from an axion signal; along with recently published results of searches for this AC osciluncertainty in the dark matter density at the source and uncertainty in modeling the magnetic field around the AGN, there are major systematics that must be accounted for. These difficulties are somewhatalleviated by using galactic pulsars as astrophysical polarization sources, as Castillo et al. [26]. Interferometric laboratory searches utilizing this polarization-rotation effect, such as DANCE [27] and ADAM-GD [28], promise significant increases in sensitivity over the current state of the art at a wide range oscillation effect to date, improving on current limits by a of masses,but such searches are in the early stages with results still many years away.

Searches using the CMB have smaller systematic uncerment with which to carry out this search. In Sec. III, the tainties than those using AGN because the polarization of the CMB has no intrinsic time variation on the experimentrelevant scales of hours to years. Compared to future laboratory searches for time-dependent birefringence, CMB experiments have datasets currently available that span many years and cover significant fractions of the skylocated at the Amundsen-ScottSouth Pole Station in The noise properties of these datasets are sufficiently well-Antarctica [31]. The currentcamera installed on the teleinteresting range of a.

Ultralight axions have two main effects on CMB instantaneouslybut rather photons decoupled over the course of ~100,000 years. In the mass range considered this work (approximately 10⁻²² eV to 10⁻¹⁹ eV, corresponding to oscillations on the order of hours to years), the pproximately 1.2 arcminutes at 50 GHz. axion field oscillates many times over the visibility function. In an ongoing multiyear, survey, SPT-3G is used to of the CMB at last scattering. This leads to an averaging slightly reduced polarization thats static in time, manifesting as a slight suppression of the CMB polarization power spectra. Second, in what F19 call the AC oscillationcentered on -44.75 deg, -52.25 deg, -59.75 deg, and effect, the oscillation of the local axion dark matter field induces a time-dependent birefringence effect, causing the telescope sweepsacross the entire RA range at a polarization angle of CMB photons to oscillate in time. large at the masses under consideration is coherent over long periods of timeAdditionally, because field, the oscillation appears in phase across the entire

effect are fundamentally limited due to cosmic variance variance that arises due to the fact that there are a finite number of modes a CMB experiment could observe from our fixed location relative to the CMB), with the current constraints a factor of ~ 7 away from this limit [20]. Therefore future discovery potential musely on the AC lation effect, demonstrating its viability as a search technique ([29,30], hereafter BK22).

In this paper, we describe a search for the AC oscillation effect using SPT-3G, the current camera installed on the South Pole Telescope (SPT), in which we measure a time series of polarization rotation angles and associated uncertainties, fit a sinusoidal model, and extract limits, on Vige set the tightest limits on axion dark matter through the AC factor of ~3.8 and approximately matching the limit from F19 proposed using the cosmic microwave background the washouteffect. In Sec. II, SPT-3G is described with (CMB) as a source with which to carry out an axion search discussion of the broader context follow in SetV.

II. INSTRUMENT AND DATASET

The SPT is a 10-meter millimeter-wavelength telescope

understood to measure time-varying birefringence across smope is SPT-3G, an array of ~16,000 polarization-sensitive transition-edge sensor (TES) bolometers [3/2]s detailed in Sobrin et al. [32], the bolometers are cooled to an measurements. The first effect (what F19 call the washoutperating temperature of 300 mK by a 3He=4He sorption effect) accounts for the fact that the CMB was not formed cooler for ~15 hours at a time, separated by a ~4.5 hour interval when the cooler is re-cycled. SPT-3G is designed to burserve the CMB in three bands, centered at approximately 95, 150, and 220 GHz, with an angular resolution of observe a ~1500 degpatch of the sky spanning -50 deg effect which causes the CMB we observe today to have ato 50 deg in right ascension (RA) and -70 deg to -42 deg in declination. The full survey field is broken up into four subfields, each spanning the full range in RA and -67.25 deg in declination. In a subset of data called a scan, constant velocity and elevation (corresponding to a nearly Because the coherence length of the local axion field is soonstant declination due to its location roughly a kilometer from the geographical South Pole). The telescope performs two scans in opposite directions (a scan pair) at the same the measured rotation is set by the local value of the axionelevation before stepping up 12.5 arcminutes; this process is then repeated until the entire declination range of a sky. CMB experiments can measure the amount of polari-subfield has been coveredThe combination of all scans zation rotation as a function of time, directly measuring theogether is called an observation. Each observation effect of the dark matter. Constraints from the washout takes approximately two hours and generates set of

time-ordered data (TOD) for each bolometer that can later be turned into maps of the sky (Sec. III A). In addition to the survey field observationsSPT-3G also takes regular (iii) calibration observations, which are described in more detail in Sobrin et al. [32] and Dutcher et al. [33] (hereafter D21).

For the work presented here, we use data from SPT-3G's 2019 observing season. Specifically, we use only the 95 GHz and 150 GHz bands, as they have the highest CMB sensitivity. Gaps between the panels of the telescope primary mirror create diffraction sidelobes, which can couple to the sun and produce stripes in the SPT-3G maps. To avoid this systematic signal, we limit ourselves to data between March 22, 2019 (sunset at the South Pole) and November 30,2019. These choices are conservative cuts motivated by an internal analysis examining the time dependence of sun contamination in the maps. As pairst calculate the power spectral density of each timeof our suite of jackknife tests (detailed in Sec. III D), we alsteam (that is, the TOD for a single bolometer for a single test the remaining data for evidence of sun contaminationscan) and determine the variance in the timestream

SPT-3G is well suited to perform a search for the AC oscillation effect. Its location at the South Pole allows it to The timestreams are inverse-variance weighte and the observe the same patch of sky regardless of the rotation of eights in map space are the sum of the weights of the the earth. The combination of a long period of observatiorspecific bolometers that are binned into each pixel (see with finely sampled individual observations allows it to be D21 for further details). These weights are used to sensitive to oscillation frequencies (and therefore axion masses)spanning more than three orders ofmagnitude. Finally, due to its high angular resolution, SPT can measure (Sec.III C). the CMB E-mode power with S=N ≥ 1 to small angular scales. In particular, SPT is sensitive to ~16 times as many modes as BK22 (which has an angular resolution of ~0.5 deg at 150 GHz), allowing it to set tighter limits than BK22 on g_{hv} by a factor of ~4 [see Eq. (24)].

III. METHODS

The analysis proceeds as followsnaps of each observation are created from the TOD (SedJ A); particularly noisy maps are cut(Sec. III B); for each observationwe calculate a polarization rotation angle and uncertainty (Sec. III C); we analyze the resulting time series of angle for systematic effects (SedII D); we then search for a periodic signal in this time series (Sedll E).

A. Time-ordered data to maps

The raw TOD from each scan are converted into CMB temperature units filtered, and binned into maps in the manner described in D21giving us the intermediate data single map per observation. There are three differences between D21 and the current work:

- (i) To reduce the amount of aliased power in the maps to cut observations with nonuniform weights, as this we set the cutoff for the low-pass TOD filter at I ¼ 5000 rather than I ¼ 6600.
- ing TOD filtering comprises all sources detected in the weights divided by the median weight for each

2018 data with a signal-to-noise ratio of greater than 10 in the 95 GHz observing band.

Lastly, although we only calculate polarization rotation angles on coadded single-observation maps, we choose to save maps ofevery individual scan rather than coadded left- or right-going maps as in D21. This allows a more detailed understanding of the statistical properties of individual observations. which provides valuable information when deciding which observations to cut. Additionally, it allows us to generate many noise realizations per observation, which is necessary to determine the uncertainty of the per-observation polarization rotation angle (see Sec.III C 4 for details).

Map-space weights are also calculated in this step. We by integrating the power between 1.0 Hz and 4.0 Hz. determine the data quality in an observation (Setll B) and coadd individual observation maps into a full season

B. Data cuts

In order to prevent particularly noisy or miscalibrated timestreamsfrom being coadded into maps, individual detectors are flagged and their TOD cut during every scan. As in D21, leading reasons detectors may be flagged are: having anomalous calibration statistics; dropping out of the superconducting transition; having too large a variance in the timestream; or being subject to large, sudden shifts (denoted glitches) in their timestreams. The only difference is that significant improvements were made to the glitchfinding algorithm between D21 and the current worlQn average per scan, in the 95 (150) GHz band, we flag 1091 (925) bolometertimestreams which leaves 3489 (3641) bolometer timestreams that are binned into the maps.

Even after flagging bad bolometer times treams some single-observation maps wilhave undesirable noise properties; for this reason, we institute additional cuts on entire maps (choosing cutoffthresholds so as to cutany clear outliers). We implement a few cuts based on the map products of one map per scan. We can then coadd (that isveights: observations with median weights below a cutoff perform a weighted average of) the per-scan maps into a threshold are cut due to their high noise level: observations with median weights above anothercutoff threshold are also cut on the basis that they are unphysical. We also want usually indicates a significant change in weather or detector

responsivity over the course of the observation. To identify (ii) The source list used for masking/interpolating dur- these observations we calculate the standard deviation of

observation, cutting any where this quantity is above a cutoff threshold. We cut all maps for observations that we frequency, δ is the phase, ϕ_0 is the maximum value of aborted early, as this usually signals an early end to the fridge cycle and thus it is assumed that the data before the We do not know the true CMB fields Qand U₀, so we performance. Finally, we construct simulated maps (see Sec. III C for details) with opposite-direction scans subtracted from, rather than coadded to, each other. The polarization rotation angles computed from these maps should be consistent with zero; thus as a final cut, we flagpower of our limits, though due to the ~250-day span of any observation where either this angle or the angle divided data, the effect is negligible for even the lowest by its uncertainty is above a cutoff threshold.

SPT-3G took 1604 observations splitacross the four subfields between our chosen start and end dates. With thetation (that is, any constant birefringence). chosen cutoff values we flag 59 observations for cutting, amounting to a 3.7% reduction in data volume.

C. Maps to angles

of the on-sky polarization rotation angle for each observation for each observing band. In terms of quantities that ifests as a rotation of the Stokes Q parameter into Stokes $U_i^{p_i}$ represents the observed Q and U maps at pixel i (and vice versa). These maps include polarized signals from $P_{Q_i}^{p_i}$ $P_{Q_i}^{p_i}$ we measure with SPT-3Gthe polarization rotation manboth the CMB and astrophysicalforegrounds; while the rotation of the foregrounds is not necessarily in phase with pixel i [given by Eq. (1)], and Çq;ij is the map-domain that of the CMB, the CMB signal is dominant over the a fair assumption that any observed time-dependebirefringence would be dominated by the rotation of polarized expression for $\hat{\rho}$ if we assume that the covariance $G_{\alpha;ij}$ CMB photons. In the limit of a small rotation amplitude, our model for the measured Q and U is

where the "m" superscript denotes modeline 0 subscript map pixel (since the rotation is the same across the entire included in the process for determining the uncertainty map), and ρ is the polarization rotation angle induced by the on $\hat{\rho}$ (Sec. III C 4). Thus we set $\partial \mathbb{Q}_{pq;ij}$ 1/4 0 for all $i \neq j$.

$$\rho_m \delta t \mbox{\vdash 1_4 A sin $\delta 2\pi ft \flat $\delta \mbox{$\triangleright$}$}$$

$$\mbox{1_4 $g_{\varphi \gamma} \varphi_0$ sin $\delta m_{\!\!\!\beta} t \flat $\delta \mbox{$\triangleright$}$; } \delta 2 \mbox{\triangleright}$$

the local axion field, and m_b is the axion mass. observation was stopped are tainted by degraded cryogenise the full-season coadded and filtered Q and U maps as estimates (further details in Sec. III C). As a consequence of this choice, all single-observation angles p are measured relative to the season-long average. For low-frequency modes, this has the effect of reducing the constraining

where A is the amplitude of the oscillation, f is

frequency we consider (0.01 inverse-days) Additionally, this means that by construction we do not measure any DC

In order to estimate p, we coadd our individual-scan maps into a single complete-observation mapWe then construct the map-space quantity

Once maps have been made, we calculate the magnitude
$$\delta p > 1/4$$
 $\delta P_{pi} - P_{pi}^m \delta p > \delta C_{pq;ij} \delta P_{qj} - P_{qj}^m \delta p > 0$; $\delta S_{pi} + P_{pi}^m \delta p > 0$; $\delta S_{pi} - P_{pi}^m$

represents the mode expectation for Stokes parameter p covariance between abixels and Q and U maps. foreground signal in the SPT-3G patch of the sky. Thus, it is The best-fit rotation angle is determined by minimizing the χ^2 with respect to ρ . We can derive an analytical is diagonal in i, j; that is, that there is no pixel-pixel covariance For maps with our chosen 2-arcminute resolution, the average pixel-pixel covariance in Q and U maps is negligible for all but a pixel's nearest neighbors, where it is approximately at the 10% leveNeglecting this covariance causes Eq. (3) to be slightly nondistributed. While this means we cannot use its asymptotic form for hypothlimit where g_{γ} ¼ 0, i represents the index of an individual to perfect the result of the resul Because our maps are inverse-variance weighted, can replace this quantity with the polarization weight matrix W (that is, $C_{pq;ii}$ 1/4 1=W_{pq;i}). Writing all terms out in explicit detail, we determine that

where the sum over i is a sum over the pixels in the map.

 $^{^{1}}$ The true on-sky rotation angle $_{
m sR}$ is related to the Q=U rotation angle by a factor of $2\!\!
ho_{
m sky}$ $^{\prime}$ 4 ho=2.

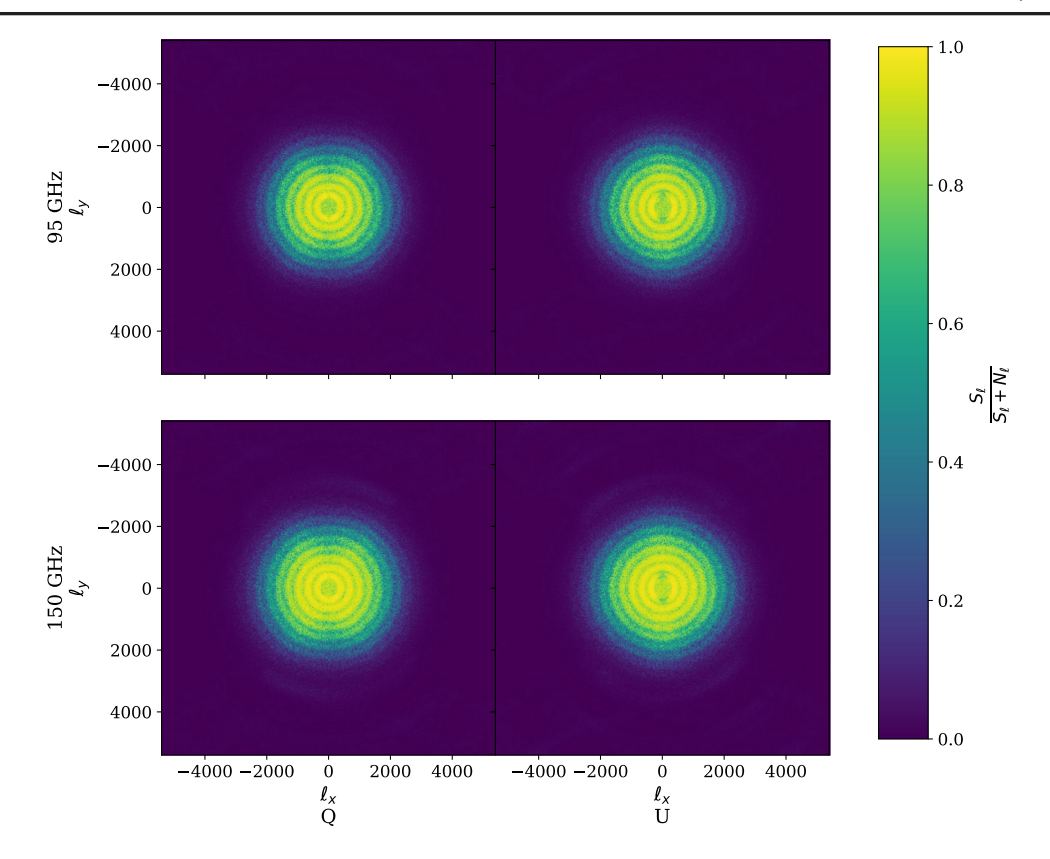


FIG. 1. I-space Wiener filter that is applied to the template coadds to downweight noisy modes. Because the noise properties of the maps differ between Stokes Q (left column) and U (right column), as well as between 95 GHz (top row) and 150 GHz (bottom row) observing bandseach mustbe filtered independently.

Because each observation takes ~2 hoursye cannot instantaneously sample the polarization rotation angle p. We assume then that our estimated angles actually an

where т is the mean time of the observath and we use the unnormalized sinc function. The effect of this averaging where the prime denotes the filtered map, denotes the ~5% at even the highest frequency we consider (2.0 inverse-days).

1. Template coadds

and U maps as estimates for the true CMB polarization fieldsight noisy modes by emphasizing modes with high Q_0 and U_0 . Although the maps are signal-dominated on signal-to-noise ratios (thats, the same modes where the most relevant scales, the noise contribution is not negligible BE power spectrum peaks). this noise biases the estimator for the angle Given the noise level of our dataset, we observe a ~50-60% reduction in the value of \hat{\rho}. To see why this bias occurs,

consider the limit where Qand U₀ are composed of only noise and no CMB. Due to the small-angle approximation made in our model any rotation adds noise power in this limit and makes the 2 larger, so is disfavored by the angle estimator.

To mitigate this bias, we apply a Wiener filter to the fullseason coadds,

Fourier transform, and S.P. and N.P. represent the twodimensional signal (i.e., CMB) and noise power spectra, respectively, for Stokes parameteP. Because the noise properties vary by Stokes parameterand by observing band, each band's Q and U maps are filtered independently.

As mentioned above, we use the full-season coadded These filters are shown in Fig1. They effectively down-

S was determined using the SPT-3G map-space simulation pipeline, which is described in brief here (see D21 for full details). In a process called mock observation fake

pointing, detectorselection, and TOD weights from an observation. These TOD are passed through the entire mabould be corrected. making pipeline to create a simulated map.

To determine \$, we created 10 noise-free, Gaussian realizations of the CMB sky, with underlying power spectra determined using the best-fit cosmological parambefore mock-observing them with a random subset of eters from thease_plikhm_ttteee_lowl_lowe_lensing observed with the pointing/detector-cutting information from three random observationsper subfield, and the resulting 12 maps were coadded together and the power < 0.1 deg; at this level the bias should be < 0.002 deg. averaged to give us S

N_I was estimated from the data themselvesusing season-long signflip noise realizations. For every observation, we subtracted the left-going map from the rightgoing one to remove the CMB signal. The resulting difference map is then assigned a random sign and the full set is coadded together ogive an estimate of the noise realizations per observing band, took the power

of the CMB, and this will leave some residual bias. We camaps. The sources' time-varying polarization powercan use the same simulation framework to test whether this bigs the estimated angles in a way thatooks like a false is at an acceptable level. We filtered a noisy template coaddon signal and causes jackknife failuresFor example, and used it to estimate angles on a collection of noisy single-observation simulated mapswith a 2.00 degree Q=U rotation injected. The distributions of reconstructed angles have mean 2.03 0.06 (2.02 0.05) the cost of a sensitivity reduction of approximately 10% (as measured by the magnitude of the uncertaintyon

There is another bias introduced by the use of the fullseason coadds the estimates for Q₀ and U₀. In the presence of a signalthe true Q and U fields are slightly angle measured in individualmaps appearlarger than it truly is. However, this is a second-order effect that is, it scales as Oodp and can be safely neglected here.

2. Mapmaking procedure bias

It is well documented that the TOD filtering biases the be accounted and corrected for in power spectrum analyses nsitivity loss of only ~1%. by determining the transfer function of the mapmaking procedure. This power spectrum bias does notbias the

TOD are generated from a simulated sky using the actualto the removal of E-modes. However, it is possible that our mapmaking procedure could introduce a bias top that

In order to test this, we again generated a set of noise-free Gaussian CMB realizationsapplying a Q=U rotation to these mock skies (arbitrarily chosen to be 2.0 degrees) observationsWe observed a slight reduction in the value 2018 Planck data release [34]. Each realization was mockef the angle we reconstructed from these maps, on the order of 2%. It is unclear what the source of this bias is, but the F19 upper limits on gplace the amplitude of rotation to be spectrum was estimated. These 10 power spectra were the cause this bias is entirely negligible when compared with the uncertainty on the angles from each observation (discussed in more detain Sec. III C 4), we elect to not correct for it. This is, however, a potential improvement to be made in future analyses of this type.

Map-space source masking

As described in Sec.III A and in more detail in D21. coadded noise for the full season. We generated 33 of the season samples where a bolometer is pointed at a point source are masked during TOD filteringThis avoids the spectrum of each, and set equal to the average spectrum. creation of artifacts from the polynominaliltering of the After filtering, Q_0 and U_0 are not perfect representations timestream but leaves the sources themselves in the output PMN 0208-512 is a bright, variable AGN in the SPT-3G survey area whose flux varies between ~1-5 Jy and produces a detectable time variation in ourpolarization angle estimatorTo account for the bias from sources like 95 (150) GHz; thus, we conclude that using a Wiener-filtered, we apply a map-space mask with a 5-arcminute radius template coadd reduces the bias caused by a noisy template sources detected above 50 mJy in a coadd of 95 GHz coadd to a negligible level. However, the filtering comes at at from SPT-3G's 2018 observing season (though the list is chosen based on source flux at 95 GHz, the same sources are masked when calculating angles forboth observing bands). Once the mask is applied, we calculated each observation. This threshold was chosen based on Henning et al. [36], which demonstrated thatsources below the washed out in the coadd, making the polarization rotation cutoff flux value contribute negligible power to polarization power spectra. We confirmed that the variance added to by leaving these dim sources unmasked is subdominant to

We end up masking ~2% of the effective sky area in the SPT-3G field. The uncertainty on the final rotation amplitude scales approximately as the inverse-square-root of the estimation of CMB power spectra [35], a bias which must sky fraction observed (Sec. IV), so this masking leads to a

4. Estimating the uncertainty on ρ̂

the intrinsic uncertainty in the estimate (Seld C 4).

estimation of; it only adds a small amount of variance due To estimate the uncertainty on the polarization rotation angle for each observation, we require a method to generate ²Washout during last scattering, as described in Sec. I, is non-any noise realizations with the statistical properties of the noise in that particular observation's map. We calculate an angle for each of these noise realization and set the

negligible because the strength of the axion field ϕ_0 is much larger during lastscattering than today.

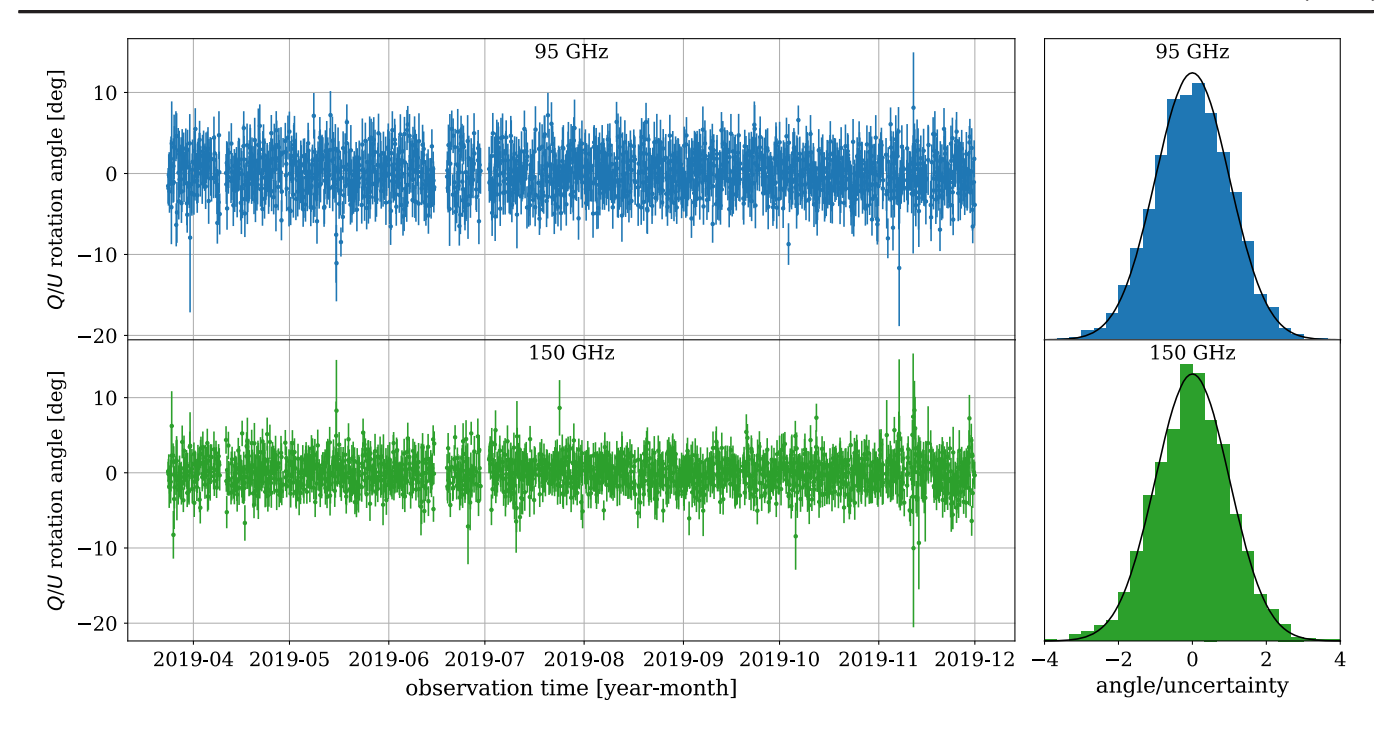


FIG. 2. (left) Time series of polarization rotation angles measured for both the 95 GHz and 150 GHz bands. The gaps where there are no angles for a short period correspond with telescope downtime due to unscheduled drive maintenance. (right) Histopprams of x 1/4 for both observing bandsh both casesthis quantity is consistent with a uniGaussianplotted as a solid black line.

uncertainty on $\hat{\rho}$ to be $\sigma_{\hat{\rho}}$, the standard deviation of the distribution of angles.

We take inspiration from the season-long signflip noise quantities that vary in time (such as whether the moon is realizations detailed in SedII C and devise a method of leaving only a noise estimate for that can pair. We then assign a random sign to each pair's noise map and coadddafference maps).

observation. We generate 1000 such realizations per obseimulated time series of polarization rotation angle sor precision. The average uncertainty orp is 2.50 deg for 95 GHz observations and 2.01 deg for 150 GHz observations as subfield as observation i and computing

With our chosen TOD filtering settingswe expectour single-observation maps to be dominated by white noise. Therefore we also expect the quantity $x \frac{1}{4} \hat{p} = \sigma_h$ to be Gaussian distributed with mean zero and standard deviation

unity. As a consistency check thatwe are estimating a correctly, we perform a Kolmogorov-Smirnov (KS) test for from the actual data; in this way we are able to create p-value on the KS test of 0.621 (0.877) for the 95 (150) G神gse of the real data. data. Because these are within the 95th percentile, we claim that x is consistent with being Gaussian-distributed The final time series of angles and uncertainties are shown for both observing bands in Fig2.

D. Jackknives

Once we have a time series of polarization rotation angles, we perform a suite of jackknife tests to search for

systematic effects in the data. These tests can be broken up into three categories: temporal jackknives, for binary

above or below the horizon); continuous jackknivesfor generating signflip noise realizations on the per-observation tinuous quantities that vary in time (such as observation level. For each scan pair, we subtract one scan from the addienuth); and null jackknives, for data combinations where we expect the signal to be nulled (such as left-right 36 scan pairs together to get a noise realization for the full All of the jackknife tests depend in some way on

vation, allowing us to determine the uncertainty with high each observation i in the fake time series e simulate an angle & randomly selecting an observation j from the

Each quantity on the right-hand side of the equation comes Gaussianity on these distributions for both bands. We find mulated time series with noise properties consistent with

1. Temporal jackknives

We use the temporaljackknife to test for systematics induced by quantities that take on one of two distinct values in each observation. Specifically, we split our time series in three ways:

(i) Sun up/down,to test for sun contamination in the data through telescope sidelobes.

- (ii) Moon up/down, to test for false signals from the periodic rise and fallof the moon.
- order to probe atmospheric effects.

In each casewe construct a likelihood

$$L \delta A; \; \delta; \; f \triangleright \; \frac{1}{4} \; exp^{-} \frac{\delta \hat{\rho}_{i} - \rho_{m;i} E^{2}}{2 \sigma_{\hat{\rho};i}^{2}} \; \equiv exp \; -\frac{\chi_{TS}^{2}}{2} \; ; \quad \delta 8 \triangleright$$

where $\rho_{\!\!\! h;i}$ ¼ A sin $\eth 2\pi f\!\!\! t b$ is the model angle [Eq. (2)] at time t and the summation is over observations; stythe time series $\frac{2}{3}$, not to be confused with the map-space $\frac{2}{3}$ introduced in Eq. (3). Then we take as a testitatistic λ , defined to be the log-likelihood ratio

$$\lambda_{t} \equiv -2 \log \frac{\max_{A_{;\bar{\delta};f}} \frac{1}{2} I_{tot} \delta A_{;\bar{\delta};f} }{\frac{1}{2} \max_{A_{;\bar{\delta}_{1}}} I_{1} \delta A_{1}; \; \bar{\delta}_{1} P^{1}_{2} \max_{X_{;\bar{\delta}_{2}}} I_{2} \delta A_{2}; \; \bar{\delta}_{2} P} ;$$

where Ltot is the likelihood of the full time series and Is the likelihood of the ith split time series. In the Li functions, the frequency has been fixed to the best-fit frequency from the full likelihood optimization, as this

caused the distribution of λ_t values to be closer to a χ^2 distribution. This frequency-fixing is a valid nested hypoth-(iii) An elevation-based test that compares data from twesis, such that the likelihood ratio continues to be an optimal different subfields, for all possible subfield pairs, in test statistic, albeit over a reduced parameter space. With this definition, λ_t will be large in cases where there is an oscillatory systematic in one of the two splits. We consider frequencies between 0.01 inverse-days and 2.00 inversedays, with a frequency spacing of 5 × 10⁴ inverse-days. This frequency spacing oversamples the frequency width of a sine wave ensuring that we are sensitive to all possible signals in the considered range. The test statistic for the data is compared to a distribution of test statistics from simulated background-only time series in order to calculate a p-value.

> Due to the frequency fixing, the temporal jackknife is only sensitive to systematics at the best-fit frequency for the full time series. We are especially interested in testing for systematicsat this frequency because this is where a potential signal is likely to appear. However, due to windowing effects (Sec.III E), and because we wish to set limits at all frequencies under consideration, we search for systematic effects at other frequencies as well. In order to do so, we also perform a variation on the temporal jackknife that we denote the noise jackknifen the noise jackknife tests, the best-fit signal is subtracted from the full time series. Then the slightly altered log-likelihood ratio

$$\lambda_{n;i} \stackrel{1}{\cancel{1}}_{4} - 2 \log \frac{\max_{A_{i}\bar{\delta}} \stackrel{1}{\cancel{1}}_{2} I_{lot} \check{\delta} A_{i}; \, \delta_{i}; \, f_{i} }{\frac{1}{\cancel{1}}_{2} \max_{A_{i},\bar{\delta}_{i}} I_{L_{1}} \check{\delta} A_{i}; \, \delta_{i}; \, f_{i} P \stackrel{1}{\cancel{1}}_{2} \max_{A_{i},\bar{\delta}_{i}} I_{L_{2}} \check{\delta} A_{2}; \, \delta_{2}; \, f_{i} P} \qquad \qquad \check{\delta} 10 P$$

is computed at all 3981 frequencies inder consideration. To pare this information down to a single p-value, we compute the test statistic, A defined as

$$\lambda_n \equiv \max_i \delta \lambda_{n,i} P;$$
 $\delta 11P$

from simulated background-only time series.

2. Continuous jackknives

SPT-3G's location athe South Pole, coupled with the fact that it observes a patch of fixed RA in the sky, means that observations are taken across the entire 2π range in azimuth. If there is a systematic induced by ground pickup This final jackknife test was developed to search for (that is, light scattering off of ground-based features)t, temporally varying quantity we cannot use the temporal jackknife since azimuth takes on continuous rathethan to test for azimuth-synchronous signals.

Before running this test, the best-fit signal in time is subtracted from the time series. We then fit a sinusoid to the time series as a function of observation azimuth rather First, a time series is constructed of angles with the than time. Its amplitude is compared to a distribution of

amplitudes from simulated background-only time series in order to calculate a p-value. We choose to look only at the fundamentalmode (that is, an azimuthal sinusoid with a period of 2π) and to neglect higher-frequency azimuthalmodes because the horizon around the SPT is mostly featureless with the exception of the Dark Sector and compare this with a distribution of similar test statisticsaboratory building where the SPT is housedAlthough this feature will not appear as a pure sine wave, the strongestcomponent of its Fourier decomposition will be the fundamental mode and thus this test is sensitive to the most likely cause of ground pickup.

3. Null jackknives

systematic signals in quantities where any true axionlike ought to show up as a function of azimuth. Though this is signal should be nulled. It is used to probe scan-directiondependentsystematic effects (as could be caused by our decision to not correct for detector time constants) as well binary values. Thus we implement the continuous jackknifes differences between the 95 GHz and 150 GHz observing bands (as could be caused by astrophysical egrounds). We do not expectany systematics in these quantitieso these tests serve as an internal consistency check. expected signal nulled. In the scan-direction case, this

involves calculating a polarization angle from maps whereor every frequency/mass bin. As stated before, we consider left-going and right-going scans have been given opposite requencies spaced 5 x 10 inverse-days aparbet ween signs. In the observing band caset involves subtracting the two time series (while adding their uncertainties in the amplitude of the best-fitsinusoid atevery frequency. Similarly to the noise jackknife, we take as a test statistic the largest of these amplitudes. A p-value is then computed insequences of his uneven sampling are discussed in by comparing with a distribution of test statistics from simulated background-only time series.

4. Jackknife results

We set two criteria to determine whether we pass our jackknife tests. First, the smallestp-value mustbe larger than 0.05=N_{ests} or 0.0014 with our 37 tests.Second,we expect the distribution of all p-values to be uniform in the absenceof systematics, so we perform a KS test for uniformity and require that the p-value on this KS test be greater than 0.05.

The full suite of p-values is presented in Table IThe smallest p-value is 0.0067 and the p-value on the KS test for uniformity is 0.4416. Thus we pass our jackknife tests and conclude that there is no evidence of strong systematic effects in the data.

E. Angles to upper limits

Once we have a time series of polarization rotation angles, the next step is to calculate upper limits on the polarization rotation amplitude. This is done independently

This is integrated to obtain a cumulative density function,

TABLE I. P-values for the full suite of jackknife tests performed to search for evidence of systematics in the time series of polarization rotation angles the minimum p-value of 0.0067 is greater than our success threshold of 0.05=N1/4 0.0014, and success threshold of 0.05. While the p-value for the 95 GHz/ 150 GHz jackknife test is unusually highlis signifies that the data are even more consistent with displaying no systematic systematic effects.

	95 GHz		150 GHz	
	Temporal	Noise	Temporal	Noise
Moon up/down	0.1865	0.5159	0.9248	0.7545
Sun up/down	0.4366	0.6819	0.4146	0.7681
e10=e11	0.3338	0.1424	0.8984	0.6317
e10=e12	0.2566	0.7275	0.0067	0.5979
e10=e13	0.0854	0.1047	0.0123	0.0808
e11=e12	0.9482	0.0746	0.7213	0.3605
e11=e13	0.4019	0.3103	0.7865	0.6122
e12=e13	0.0828	0.4516	0.7932	0.4133
Azimuthal	0.6066		0.0271	
Null	0.0655		0.8561	
95 GHz/ 150 GHz	0.9992			

0.01 inverse-days and 2.00 inverse-days (on terms of oscillation period, between 12 hours and 100 days)Our quadrature). Once we have the null time series, we computed a points are unevenly spaced roughly 2 hours apart and span a range of just over 250 days, allowing us to sample the full oscillation over the course of the season (the Sec.III E 1).

> To set an upper limit at a fixed frequency f₀, we first construct a likelihood like the one defined in Eq. (8), except that the sum is over all observations and observing bands. That likelihood is marginalized over the phase δ .

$$L_{m}$$
 $\delta A \triangleright \frac{Z}{2\pi}$ $L \delta A; \delta; f_{0} \triangleright d\delta$: $\delta 12 \triangleright$

We assume a uniform prior on amplitude with A max 1/4 0.5 ded.

$$\tilde{P}$$
ðAÞ $\frac{1}{A_{max}}$; $0 < A < A_{max}$; 0 13Þ 0 ; otherwise;

and use this prior to construct a posterior probability distribution.

the p-value on a KS test for uniformity is 0.4416, greater than our success threshold of 0.5. While the p-value for the 95 GHz/ (taken to be 0.95 here). The upper limits set by this analysis, as well as the background-only model contours, are shown signal than expected. Therefore we find no evidence of significant Fig. 3. The median expected limit is nearly constant as a function of frequency, but degradesslightly at higher frequencies due to a changing rotation angle over the course of the ~2-hour observation [Eq. (5)]. As described in Sec. III C, the limit would also degrade for low frequencies, though we do not consider any frequencies low enough for this to take effect. Below 1.00 inverse-days, where the effect of averaging is negligible (thatis, ≤1%), we set a median limit of

$$\tilde{A}$$
 < 0.142 deg; \tilde{b} 16

corresponding to $\frac{1}{2}$ < 0.071 deg.

³As long as the upper bound on the prior is high enough, the result is insensitive to the exact choice since the weight is concentrated allow amplitude.

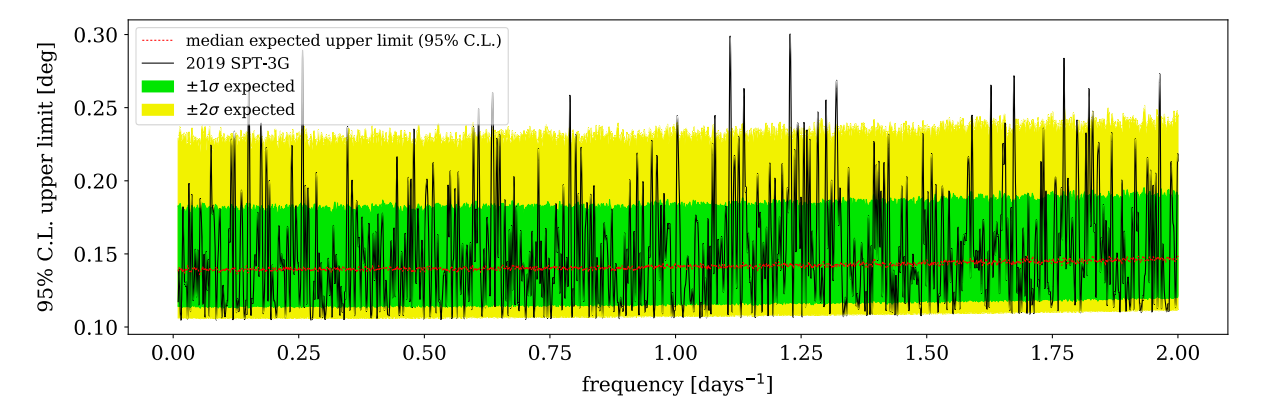


FIG. 3. 95% C.L. upper limits on Q=U rotation angle as a function of oscillation frequency (solid black line), along with simulated background-only median behavior (red) and 1σ (green) and 2σ (yellow) regions. As described in Sec. III C, averaging over the course an observation leads to less stringent limits as the oscillation frequency increases. However, this is a small effect; it is on the order of ~5% at 2.00 inverse-days. Due to the large number of frequency bins, we expect some limits in excess of the 2σ background contour; this does not necessarily constitute evidence for a sinusoidal polarization rotation.

1. Observation window function

During the course of the season, observations do not are not uniformly spaced. Although observations occur on the window function will be subdominanto noise.

scheduled cadence between recharging the sorption cooler every ~19.5 hours the schedule within this period combines CMB subfield observations with differentypes of calibration observations and the frequency with which each subfield was observed was furthermore adjusted throughout the season. In our likelihood analysis, the irregular sampling behaves similarly to a window function $\center{2}$ that is convolved with sinusoidal signals in the data. Since the sampling is notuniform, the window function can in principle have powerat any frequency, unlike the Dirac comb window function that corresponds to uniform sampling. When convolved with a sinusoid at a fixed frequencies at the sample of This base is a sinusoid at a fixed frequencies. other than f. This behavior is well documented in similar methods that identify sinusoidal signals in irregularly sampled data, such as the Lomb-Scargle periodogram [37].

While this windowing phenomenon does affect our analysis, it can be practically neglected because of the structure of the SPT-3G window function. The window function (in amplitude) of the observation times is given by

$$\begin{tabular}{lll} W \'of \triangleright $\frac{\text{X}^{N}}{4}$ exp \'o-2\pi if f_{i} \triangleright; & $\circ 17$ \triangleright \\ \hline \end{tabular}$$

where the tare the times of the N observations in our datasetand f is frequency. Figure 4 shows the window lobe and two symmetric sidelobes at the level of 14% of the servations that ccur between them in time. In an analysis main lobe in amplitude. The analysis would therefore have uch as ours without a large expected signal, the presence to detect a signal at high significance before sidelobes were sidelobes atthis level does not impact the interpretation of to be detectable, and these sidelobes furthermore would our results.

occur at predictable frequency offsets from the main signal. Given the existing constraints from the Planck washout occur at equally spaced intervals in time, so the times that analysis [20], we do not expect to detect a signal with high we assign to polarization angles in the likelihood of Eq. (8) ignificance in the present work, and any sidelobes due to

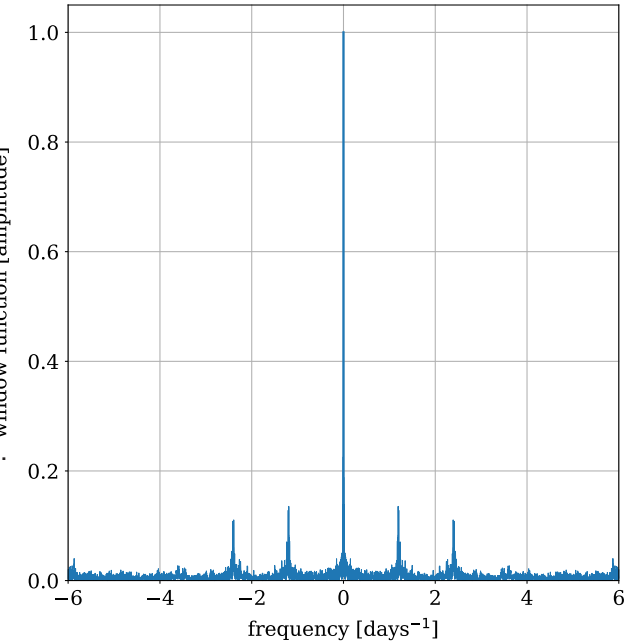


FIG. 4. Window function (in amplitude) of the observation times used in this analysis, which characterizes the extento which signals at a single frequency produce detectable power at other frequencies in our likelihood analysis. The largest sidelobes function for our data. The majority of power is in the central equasiperiodic pattern of sorption refrigerator cycles and

One further possible impact of the window function structure is that systematics that induce oscillation of the polarization angle at frequencies outside our search bandations comprise the fullfraction of the dark matter, this 0.01 inverse-days to 2.00 inverse-days could have sideloheshslates to that appear as signals inside our search band. The jackknife tests described in Sec. III D, however, are sensitive to these in-band sidelobes from out-of-band systematic effects, the impact of this phenomenon is only to complicate the physical interpretation of failures of the jackknife tests.

IV. RESULTS AND DISCUSSION

Although the 95% C.L. data limit in Fig. 3 exceeds the is not necessarily evidence of a time-varying birefringence imit is approximately flat, we take the approximation in signal due to the large number of frequency bins under consideration. We testfor detection of such a signaln a similar manner to BK22. For each frequency f_i, we compute the quantity

$$\Delta \chi^2_{TS;i}$$
 ½ χ^2_{TS} ð0; 0Þ $-\frac{2}{7}$ ξ_{i} ; ðA₀; δ_i Þ; ð18Þ

x² for that frequency bin. We take as a test statistic

A p-value testing for consistency with background is then determined by comparing, a from data with a distribution of similar test statistics computed from background-only simulations. Using this method, we find that the data are consistent with the background-only model with a p-value of 0.48.

The upper limit on rotation amplitude can be converted into an upper limit on the axion-photon coupling constant where n is the combined noise levefor all bands in the g_{bv} following the method in F19:

where A is the measured upper limit on Q=U rotation amplitude in radians, k is the fraction of local dark matter comprising axions and ρ_0 is the density of the local dark matter field. Recalling the degradation in sensitivity at higher frequencies due to the noninstantaneous sampling SPT-3G noise leveland the fact that BK22 used a somethe polarization rotation angle [Eq. (5)], we can fit a smoothed approximation to these limits of the form

determined limit\$\tilde{A}\$, we find \$\tilde{A}\$ \(\frac{1}{4} \) 0.151 deg. If we assume that the local dark matter density is 0.3 GeV³cand that

$$g_{\phi\gamma}^{ese} < 1.25 \times 10^{-12} \text{ GeV}^{-1} \times \frac{m_{\phi}}{1.0 \times 10^{-21} \text{ eV}}$$

$$\times \text{ sinc } \frac{m_{\phi}}{1.72 \times 10^{-19} \text{ eV}} \stackrel{-1}{:} \qquad \text{§225}$$

This limit on $g_{\phi\gamma}$ is shown for our results, along with other relevantimits in this region of parameter spacen 2σ background contour in a number of frequency bins, thiξig. 5. For frequencies below 1.00 inverse-days, where the Eq. (16) to set a median limit of

With a single year of data, SPT-3G sets the strongest limit yet using the AC oscillation effect, approximately 3.8 (3.4) where the subscript 0 signifies the value that minimizes themes stronger than BK22 for the flat (complete) region. At some masses this work sets the strongest limit of any CMB analysis yet, surpassing the washout limit set with Planck polarization power spectra [20].

> As a consistency checkive model the expected sensitivity difference between BK22 and the current work. In a simplified model, we expect the uncertainty to scale as

$$\sigma_{\rho} \propto n \times f_{sky}^{-1=2} \times X$$
 $C_{l} B_{l} \delta 2l \not p 1 \not p$ $^{-1=2}$; $\delta 24 \not p$

coadded template map,f sky is the fraction of the sky observed, and the final term is a scaling factor related to the size of the beam (and therefore the number of polarization modes each experiments sensitive to). For BK22, the sky area is 400 deg and n (in temperature) is approximately 1.8 µK-arcmin [43]; for this work, the sky area is 1500 deg and estimates accurate at the ~10% level place n at 4.4 µK-arcmin. Finally, the current work is sensitive to approximately 16 times as many modes as BK225iven this, our toy model predicts SPT-3G to set a limit 3.2 times stronger than BK22. Given the differences in analysis methods between the two limits, the uncertainty in the what reduced set of data when compared with [43], we find the true relative sensitivity to be in good agreementith this simple estimate.

When comparing these limits with others in the same region of parameter space, it is important to keep in mind that the limits set by F19, BK22, and the current work

with A₀ as a free parameter and Δt ½ 2.13 hours the meaassume that the local dark matter is composed entirely of a observation duration Performing a least-squares fit to the single species of axion. If instead there are multiple axions,

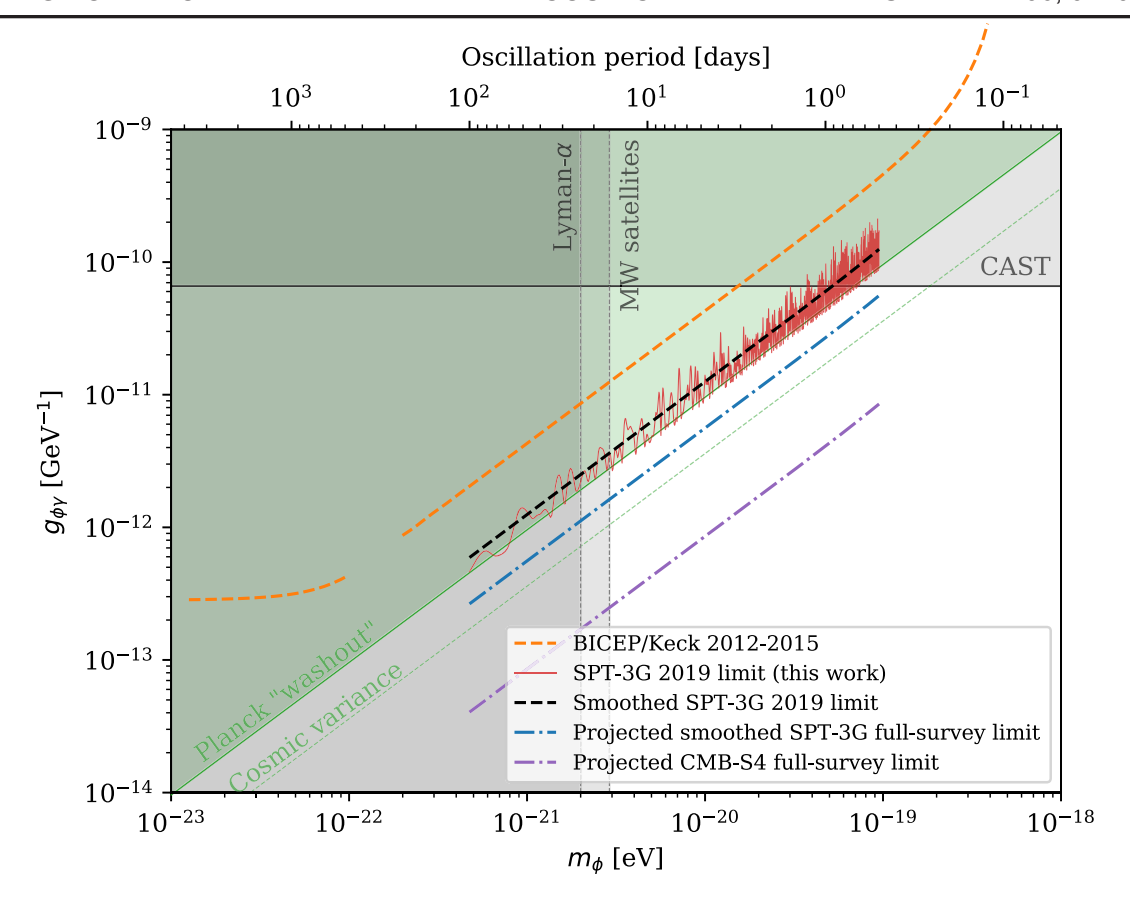


FIG. 5. The parameter space for axion-photon couplings a function of axion mass. The SPT-3G 95% C.L. upper limit is given by the solid red line, and the smoothed fit to this [Eq. (22)] by the dashed black line. The dashed orange lines represent the most rece limits set by the BICEP/Keck collaboration [30] using the AC oscillation effect; the solid green line represents the limit set with Planck data using the washout effect, with the dashed green line providing the strongest possible limit that could be set with the washout effe due to cosmic variance [20]. Projected limits using the AC oscillation effect for the full SPT-3G survey as well as the future CMB-S4 survey are given by the dot-dashed blue and purple lines, respectively (although these projections do not account for the wider mass range that full survey analyses could constrain). The CAST limit[on] gs given by the horizontal gray line (stronger limits set using data from the supernova SN1987A [38], and Chandra X-ray spectroscopy [39] are excluded from the plot as a result of difficult-toquantify modeling uncertainties). Lower mass limits from observations of Lyman-α emission [40] and Dark Energy Survey observation of Milky Way satellite galaxies [41] are given by the labeled vertical dashed gray lines (while stronger limits from Lyman-α observation exist [42], we have chosen to plot a more conservative limit). Both the BICEP/Keck and the SPT-3G results assume that axions comp the entirety of the local dark matteand thatthe density of the locablark matter field is 0.3 GeV=cm

or a single type of axion makes up only a fraction of the local abundance the limits become less stringent. The CAST limit [17] is set strictly by Primakoff conversion of solar axions and is thus independent any properties of local dark matter. While stronger limits on have been set in this mass range by observations of the supernova SN1987A [38] and Chandra X-ray spectroscopy [39], these limits are subject to large uncertainties stemming from source luminosity and magnetic field modelingnd set by small-scale structure [44], Lyman-α emission [40,42], and Milky Way satellite galaxies [41] are wholly independent of the axion details, and only assume that ardashed lines in Fig. 5. Due to the cosmic variance limit matter, they could take on masses below this limit.

We reiterate that the current work uses only a single year of SPT-3G data. Since the sensitivity scales roughly as the inverse-square-root f the number of observations, we expect that a future analysis of this type using the full 5-year SPT-3G dataset will improve the limits by more than a factor of two (as well as extend to a lower frequency range due to the longer observing time). Looking further ahead, the CMB field will begin capturing data with nextgeneration experiments such as Simons Observatory and are thus excluded from the plot. Conversely, the mass lim@MB-S4. These experiments are expected to be much more sensitive to AC birefringence-type effects; estimatesof such future limit-setting abilities are shown with the dotultralight particle is the principle dark matter component. Ibn axion searches using the polarization washout effect, it the axions comprise some subdominant fraction of the daix the AC oscillation effect that will provide the strongest constraining power from CMB data on this type of

measurement. Given that this is a relatively open region of STFC). The IAP authors acknowledge suppoftom the parameterspace, this means that there is a significant discovery potential in the future.

ACKNOWLEDGMENTS

National Science Foundation (NSF) through Grants No. PLR-1248097 and No. OPP-1852617. Partial support Student Research (SCGSR) Program. The Melbourne No. PHY-1125897 to the Kavlilnstitute of Cosmological and the Gordon and Betty Moore Foundation through Grant No. GBMF#947 to the University of Chicago. Argonne National Laboratory's work was supported by the U.S. Department of Energy, Office of High Energy User Facility managed by the Fermi Research Alliance. LLC, was supported under Contract No. DE-AC02-07CH11359. The Cardiff authors acknowledge support from the UK Science and Technologies Facilities Council stack [47–49].

Centre National d'Études Spatiales (CNES). M. A. and J. V. acknowledge supporfrom the Center for AstroPhysical Surveys at the National Center for Supercomputing Applications in Urbana, IL. J. V. acknowledgessupport The South Pole Telescope program is supported by the from the Sloan Foundation.K. F. acknowledges support from the Department of Energy Office of Science Graduate is also provided by the NSF Physics Frontier Center Grant uthors acknowledge support from the Australian Research Council's Discovery Project scheme (NDP210102386). Physics at the University of Chicago, the Kavli Foundation, the McGill authors acknowledge funding from the Natural Sciences and Engineering Research Council Canada, Canadian Institute for Advanced Research, and the Fonds de recherche du Qabec Nature ettechnologies. The UCLA and MSU authors acknowledge support from NSF Physics, under Contract No. DE-AC02-06CH11357. WorkAST-1716965 and CSSI-1835865. This research was done at Fermi National Accelerator Laboratory, a DOE-OS, HEPsing resources provided by the Open Science Grid [45,46], which is supported by the NSF Grant No. 1148698, and the U.S. Departmentof Energy's Office of Science. The data analysis pipeline also uses the scientifichon

- [1] M. Persic, P. Salucci, and F. Stel, The universal rotation curve of spiral galaxies—I. The dark matter connection, Mon. Not. R. Astron. Soc. 281, 27 (1996).
- [2] K. Garrett and G. Dūda, Dark matter: A primer, Adv. Astron. 2011. 968283 (2011).
- [3] S. Weinberg, A New Light Boson?, Phys. Rev. Lett. 40, 223
- [4] F. Wilczek, Problem of Strong P and T Invariance in the Presence of Instanton®, hys. Rev. Lett. 40, 279 (1978).
- [5] R. D. Peccei and H. R. Quinn, CP Conservation in the Presence of Pseudoparticles Phys. Rev. Lett. 38, 1440 (1977).
- [6] R. D. Peccei and H. RQuinn, Constraints imposed by CP conservation in the presence of pseudoparticles, Phys. Rev. D 16, 1791 (1977).
- [7] J. Preskill, M. B. Wise, and F. Wilczek, Cosmology of the invisible axion, Phys. Lett. 120B, 127 (1983).
- [8] L. F. Abbott and P. Sikivie, A cosmological bound on the invisible axion, Phys. Lett. 120B, 133 (1983).
- [9] M. Dine and W. Fischler, The not-so-harmless axion, Phys. Lett. 120B, 137 (1983).
- [10] L. D. Duffy and K. van Bibber, Axions as dark matter particles, New J. Phys. 11, 105008 (2009).
- [11] P. W. Graham, I. G. Irastorza, S. K. Lamoreaux, A. Lindner, and K. A. van Bibber, Experimental searches for the axion[21] W. Hu, R. Barkana, and A. Gruzinov, Fuzzy Cold Dark and axion-like particles, Annu. Rev. Nucl. Part. Sci. 65, 485
- [12] E. Witten, Some properties of O(32) superstrings Phys. Lett. 149B, 351 (1984).

- [13] A. Arvanitaki, S. Dimopoulos, S. Dubovsky, N. Kaloper, and J. March-Russell, String axiverse, Phys. Rev. D 81, 123530 (2010).
- [14] M. Cicoli, M. Goodsell, and A. Ringwald, The type IIB string axiverse and its low-energy phenomenology, J. High Energy Phys.10 (2012) 146.
- [15] J. A. Frieman, C. T. Hill, A. Stebbins, and I. Waga, Cosmology with Ultralight Pseudo Nambu-Goldstone Bosons, Phys. Rev. Lett. 75, 2077 (1995).
- [16] L. Amendola and R.Barbieri, Dark matter from an ultralight pseudo-Goldsone-bosonPhys. Lett. B 642, 192 (2006).
- [17] V. Anastassopoulos, Aune, K. Barth et al., New CAST limit on the axion-photon interaction, Nat. Phys. 13, 584 (2017).
- [18] C. Bartram, T. Braine et al. (ADMX Collaboration), Search for Invisible Axion Dark Matter in the 3.3-4.2 µeV Mass Range, Phys. Rev. Lett. 127, 261803 (2021).
- [19] L. Zhong, S. Al Kenany, K. M. Backes et al., Results from phase 1 of the HAYSTAC microwave cavity axion experiment, Phys. Rev. D 97, 092001 (2018).
- [20] M. A. Fedderke, P. W. Graham, and S. Rajendran, Axion dark matter detection with CMB polarization, Phys. Rev. D 100,015040 (2019).
 - Matter: The Wave Properties of UltralighParticles, Phys. Rev.Lett. 85, 1158 (2000).
- [22] E. G. M. Ferreira, Ultra-light dark matter, Astron. Astrophys. Rev. 29, 7 (2021).

- [23] P. Sikivie, in Axions, edited by M. Kuster, G. Raffelt, and B. Beltrán (Springer, Berlin, Heidelberg, Heidelberg, Germany, 2008), Vol. 741, p. 19, 10.1007/978-3-540-73518-2 2.
- [24] D. Horns, L. Maccione, A. Mirizzi, and M. Roncadelli, Probing axionlike particles with the ultraviolet photon polarization from active galactic nuclein radio galaxies, Phys.Rev.D 85, 085021 (2012).
- [25] M. M. Ivanov, Y. Y. Kovalev, M. L. Lister, A. G. Panin, A. B. Pushkarev, T. Savolainen, and S. V. Troitsky, Constraining the photon coupling of ultra-light darkmatter axion-like particles by polarization variations of parsec-scale jets in active galaxies, Cosmol. Astropart. Phys. 02 (2019) 059.
- [26] A. Castillo, J. Martin-Camalich, J. Terol-Calvo, D. Blas, A. Caputo, R. Tanausúe6óva Santos, L. Sberna, M. Peel, and J. A. Rubiño-Martín, Searching for dark-matter waves with PPTA and QUIJOTE pulsarpolarimetry, J. Cosmol. Astropart. Phys. 06 (2022) 014.
- [27] Y. Michimura, Y. Oshima, T. Watanabe, T. Kawasaki, H. Takeda, M. Ando, K. Nagano, I. Obata, and T. Fujita, ment, J. Phys. Conf. Ser. 1468, 012032 (2020).
- [28] K. Nagano, H. Nakatsuka, S. Morisaki, T. Fujita, Y. Michimura, and I. Obata, Axion dark matter search using arm cavity transmitted beams of gravitationwave detectors.Phys.Rev.D 104, 062008 (2021).
- [29] P. A. R. Ade, Z. Ahmed et al. (BICEP/Keck Collaborations), BICEP/Keck XII: Constraintson axionlike polarization oscillations in the cosmic microwave backgroundPhys. Rev.D 103, 042002 (2021).
- [30] P. A. R.Ade, Z. Ahmed, M. Amiri et al., BICEP/K e c k XIV: Improved constraints on axionlike polarization oscillations in the cosmic microwave backgroundPhys. Rev.D 105, 022006 (2022).
- [31] J. E. Carlstrom, P. A. R. Ade, K. A. Aird et al., The 10 meter south pole telescope, Publ. Astron. Soc. Pac. 123, 568
- [32] J. A. Sobrin, A. J. Anderson, A. N. Bender et al., The design6] I. Sfiligoi, D. C. Bradley, B. Holzman, P. Mhashilkar, S. and integrated performance of SPT-3G, Astrophys. J. Suppl. Ser.258, 42 (2022).
- [33] D. Dutcher, L. Balkenhol, P. A. R. Ade et al., Measurements of the E-mode polarization and temperature-E-mode correlation of the CMB from SPT-3G 2018 data, Phys. Rev.D 104, 022003 (2021).
- [34] N. Aghanim, Y. Akrami et al. (Planck Collaboration), Planck 2018 results. VI. Cosmological parameters, Astron[48] E. Jones, T. Oliphant, P. Peterson et al., SciPy: Open source Astrophys.641, A6 (2020).
- [35] E. Hivon, K. M. Górski, C. B. Netterfield, B. P. Crill, S. Prunet, and F. Hansen, MASTER of the cosmic microwave background anisotropy power spectrum: A fast method for

- statistical analysis of large and complex cosmic microwave background data set strophys. J. 567, 2 (2002).
- [36] J. W. Henning, J. T. Sayre, C. L. Reichardt et al., Measurements of the temperature and E-mode polarization of the CMB from 500 square degrees of SPTpol data, Astrophys. J. 852, 97 (2018).
- [37] J. T. VanderPlasInderstanding the lomb-scargle periodogram, Astrophys. J. Suppl. Ser. 236, 16 (2018).
- [38] A. Payez, C. Evoli, T. Fischer, M. Giannotti, A. Mirizzi, and A. Ringwald, Revisiting the SN1987A gamma-ray limit on ultralight axion-like particles, J. Cosmol. Astropart. Phys. 02 (2015) 006.
- [39] C. S. Reynolds, M. C. D. Marsh, H. R. Russell, A. C. Fabian, R. Smith, F. Tombesi, and S. Veilleux, Astrophysical limits on very light axion-like particles from Chandra grating spectroscopy oNGC 1275, Astrophys. J. 890, 59 (2020).
- [40] V. Iršič, M. Viel, M. G. Haehnelt, J. S. Bolton, and G. D. Becker, First Constraints on Fuzzy Dark Matter from Lyman-α Forest Data and Hydrodynamical Simulations, Phys.Rev.Lett. 119, 031302 (2017).
- DANCE: Dark matter axion search with riNg cavity experi-[41] E. O. Nadler, A. Drlica-Wagner, K. Bechtol et al., Constraints on Dark Matter Properties from Observations of Milky Way Satellite Galaxies, Phys. Rev. Lett. 126, 091101 (2021).
 - [42] K. K. Rogers and H. V. Peiris, Strong Bound on Canonical Ultralight Axion Dark Matter from the Lyman-Alpha Forest, Phys.Rev.Lett. 126, 071302 (2021).
 - [43] P. A. R.Ade et al. (BICEP2 Collaboration, Keck Array Collaboration), Constraints on Primordial Gravitational Waves Using Planck, WMAP, and New BICEP2/Keck Observations through the 2015 Season Phys. Rev. Lett. 121, 221301 (2018).
 - [44] L. Hui, J. P. Ostriker, S. Tremaine, and E. Witten, Ultralight scalarsas cosmologicaldark matter, Phys. Rev. D 95, 043541 (2017).
 - [45] R. Pordes et al., The open science grid, J. Phys. Conf. Ser. 78, 012057 (2007).
 - Padhi, and F. Wurthwein, The pilot way to grid resources using glideinWMS, in Proceedings of the 2009 WRI World Congress on Computer Science and Information Engineering (IEEE, 2009), Vol. 2, pp. 428-432, 10.1109/ CSIE.2009.950.
 - [47] J. D. Hunter, Matplotlib: A 2D graphics environment, Comput. Sci. Eng. 9, 90 (2007).
 - scientific tools for Python (2001) http://www.scipy.org/.
 - [49] S. van der Walt, S. Colbert, and G. Varoquaux, The NumPy array: A structure for efficient numerical computation, Comput. Sci. Eng. 13, 22 (2011).